

Cite this: *Chem. Sci.*, 2025, 16, 22394

All publication charges for this article have been paid for by the Royal Society of Chemistry

Molecular-level insight into the multiple mechanistic pathways in iron-catalysed alkene dimerisation

 Joseph H. P. Cockcroft,^a Annabel Flook,^a Patrick J. Boaler,^a Gary S. Nichol,^a Jarle Holt,^b Joost Smit,^b Jennifer A. Garden^b*^a and Stephen P. Thomas^b*^a

As the least expensive, least toxic and most abundant of the first-row transition metals, iron catalysis underpins the future of sustainable synthesis. Yet the mechanistic understanding remains limited, particularly for pathways involving low oxidation-state intermediates. The reductive dimerisation of alkenes is a prime example, with very few iron-catalysed examples reported and with no in-depth mechanistic analyses. As simple, 1,2-disubstituted alkenes, methyl crotonates can be selectively dimerised to 2-ethylidene-3-methylpentanedioates with two stereogenic units. This rare non-arene example of a C(sp²)-H functionalisation offers a platform for molecular-level understanding of broad scope iron-catalysed C-H functionalisation. In-depth mechanistic studies of this dimerisation, including the speciation of [(dmpe)₂FeH₂] through a combination of X-ray diffraction, kinetic analysis and *in situ* NMR monitoring, has uncovered hidden pathways that show this “simple” dimerisation is in fact a mechanistically complex system.

Received 26th September 2025

Accepted 22nd October 2025

DOI: 10.1039/d5sc07490h

rsc.li/chemical-science

Introduction

Alkenes are pivotal building blocks across small molecules and macromolecules, with key applications in commodity chemicals alongside polyolefin and polyacrylate materials.^{1–4} With increasing limitations on the use and supply of precious metals,⁵ it is vital that the chemical transformation of alkenes transitions to Earth-abundant metal catalysts. While the Earth-abundant metal-catalysed polymerisations of alkenes have been well-established,^{6,7} the linear and cyclic dimerisation of alkenes remains underexplored.^{8–12} Mechanistic understanding of Earth-abundant metal-catalysed functionalisation reactions is key to designing more efficient catalysts yet has been limited so far by difficulties in observing and isolating low oxidation-state intermediates. This in turn limits the industrial scalability of Earth-abundant metal-catalysed processes, presenting a key scientific challenge.

Methyl crotonate **1** is an alkene monomer that, unlike its methyl methacrylate isomer, does not readily polymerise under radical or anionic conditions.^{13,14} Unlike the dimerisation of similar alkenes,^{9,15} the iron-catalysed dimerisation of methyl crotonate **1** to (*E*),(*Z*)-2-ethylidene-3-methylpentanedioate **2** is limited to a single report from Komiya and co-workers which

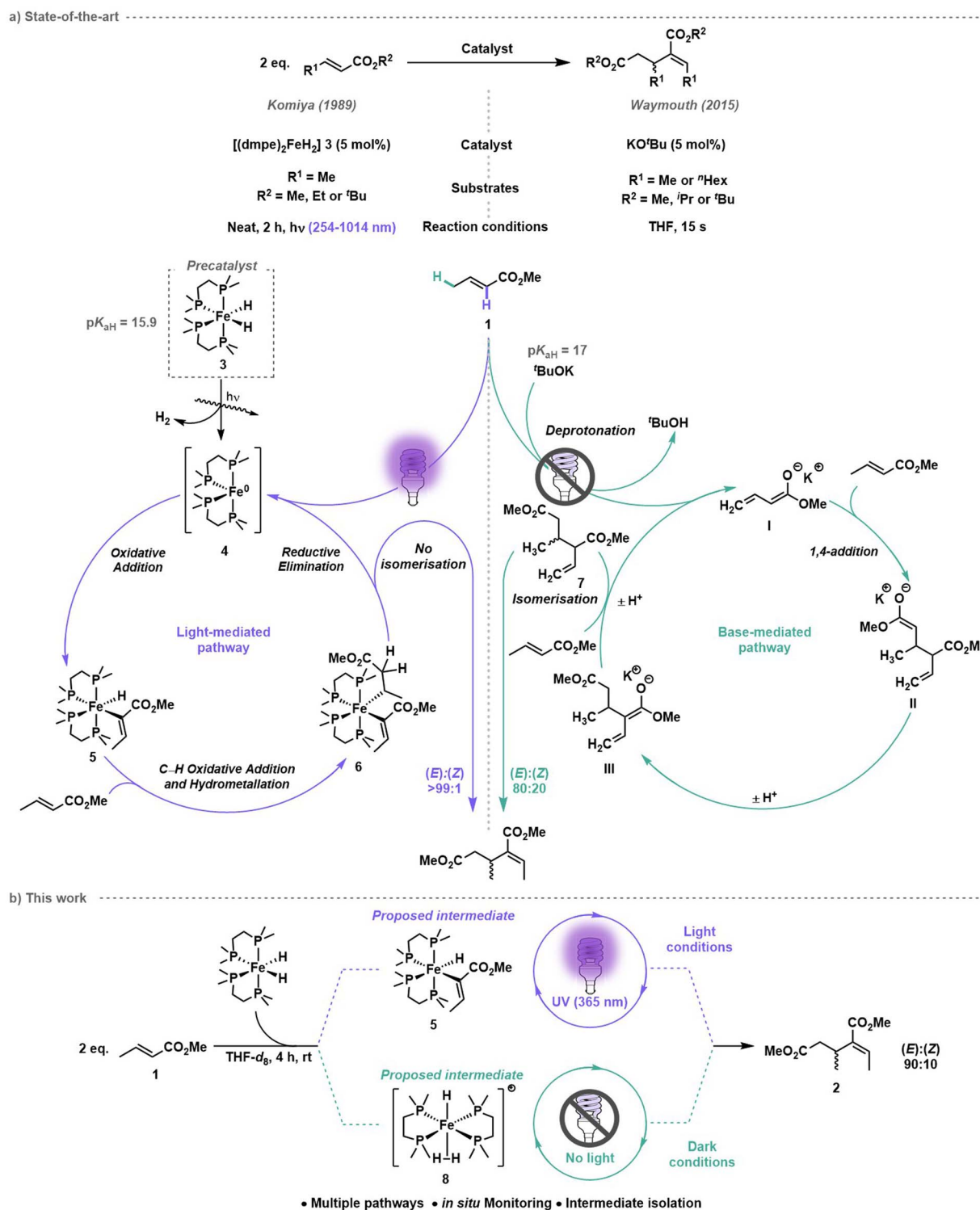
used [(dmpe)₂FeH₂] (dmpe = 1,2-bis(dimethylphosphino)ethane) **3**. [(dmpe)₂FeH₂] **3**, which has been shown to exist in the *cis*-configuration in solution by ¹H NMR spectroscopy¹⁶ (see also SI S2.2 for further details) presumably following *cis-trans* isomerisation which may or may not be light mediated, has exhibited high reactivity for the metalation and onward reaction of C(sp)-H,¹⁷ C(sp²)-H¹⁸ and even C(sp³)-H¹⁹ bonds.^{20–22} Although some mechanistic studies have been reported for iron-catalysed C-H functionalisation reactions using [(dmpe)₂FeH₂] **3**,^{21,23,24} the proposed short-lived iron(0) intermediates are notoriously difficult to identify, characterise and isolate, and this is further complicated when simultaneous irradiation and analysis is required.

Komiya and co-workers proposed that the first step of the mechanism for iron-catalysed crotonate dimerisation was the photoirradiation of [(dmpe)₂FeH₂] **3** to trigger reductive elimination of dihydrogen to form [(dmpe)₂Fe⁰] **4** (Scheme 1a, left).²⁶ Subsequent oxidative addition of the alkenyl α-C(sp²)-H bond to the ester formed an iron monohydrido-monoalkenyl species [(dmpe)₂FeH(CH₃CH=CCO₂Me)] **5**, in analogy to tetra-kis(phosphine) ruthenium complexes undergoing C(sp²)-H alkenyl insertion of methacrylates as reported by Yamamoto, Ibers and co-workers.²⁵ Insertion of a second methyl crotonate **1** into [(dmpe)₂FeH(CH₃CH=CCO₂Me)] **5** generated the hydro-metallation product, iron monoalkyl-monoalkenyl species [(dmpe)₂Fe(CH₃CH=CCO₂Me)(CH₃CH-CH₂CO₂Me)] **6**. Reductive elimination reformed [(dmpe)₂Fe⁰] **4** and a >99 : 1 (*E*) : (*Z*) mixture of 2-ethylidene-3-methylpentanedioate **2**.²⁶

^aEaStCHEM School of Chemistry, Joseph Black Building, The University of Edinburgh, David Brewster Road, Edinburgh, EH9 3FJ, UK. E-mail: J.Garden@ed.ac.uk; stephen.thomas@ed.ac.uk

^bJohnson Matthey, Technology Centre, Princeton Drive, Stockton-on-Tees, TS17 6PY, UK





Scheme 1 (a) Crotonate dimerisation by iron-catalysed (Komiya and co-workers) and base-catalysed (Waymouth and co-workers) methods. (b) This work: mechanistic investigation of methyl crotonate dimerisation using [[dmpe]₂FeH₂] 3 as pre-catalyst under light and dark conditions.

Waymouth and co-workers reported the base-catalysed reductive dimerisation of alkyl crotonates without any photo-irradiation using potassium *tert*-butoxide to achieve high yields and 80 : 20 (*E*) : (*Z*) stereoselectivity.²⁷ Using methyl crotonate as an example, Waymouth proposed δ -C–H deprotonation (C(sp³)-

H bond) gave the (extended) enolate I (Scheme 1a, right). 1,4-Addition of I to another molecule of methyl crotonate 1 gave an anionic dimer II, which underwent proton transfer to give the conjugated enolate III, which deprotonated a third methyl crotonate 1 to regenerate enolate I as well as forming dimethyl



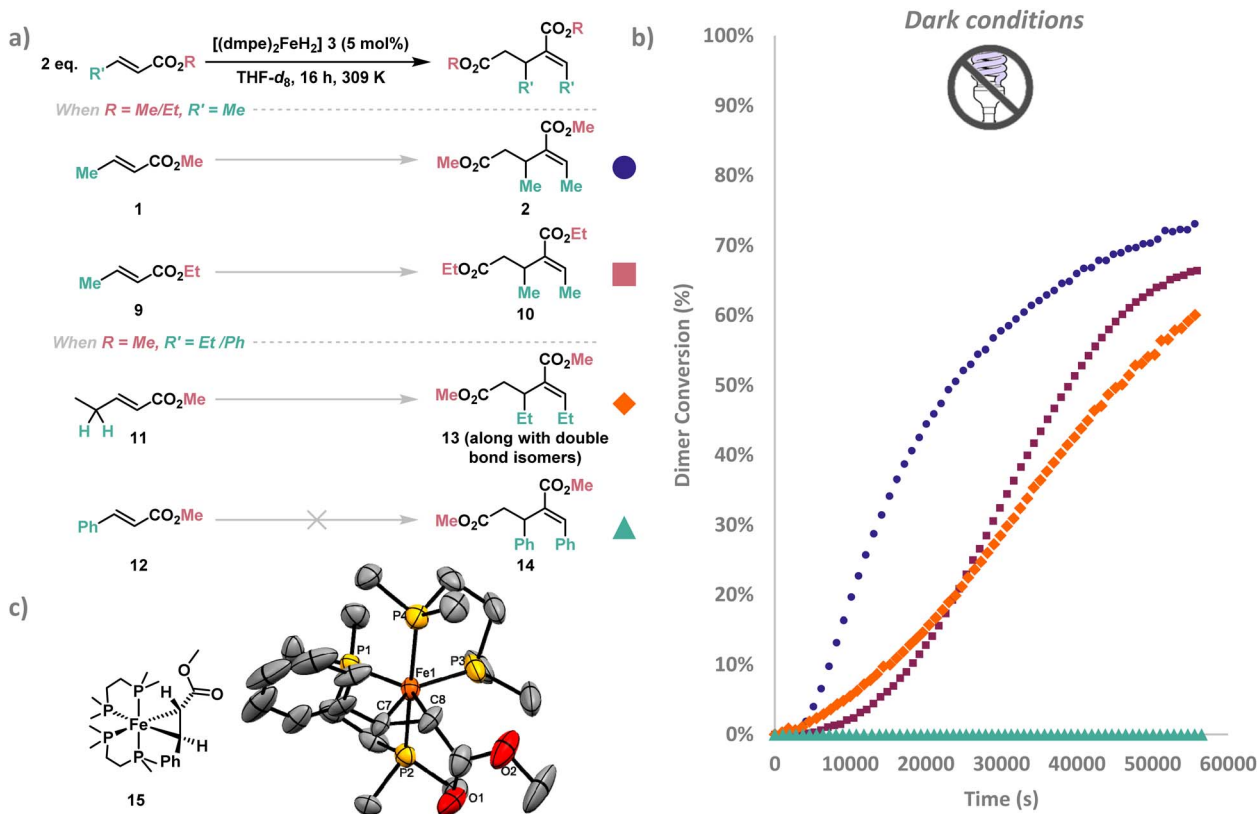


Fig. 1 (a) *in situ* Monitoring of crotyl substrates **1**, **9**, **11** and **12** under dark conditions with $[(dmpe)_2FeH_2]$ **3** (5 mol%) in $THF-d_8$ at 309 K were converted to dimers **2**, **10**, **13** and **14** respectively. The substrates selected either had a different alkyl ester ($R = Me, Et$) or different substituents at the vinylogous position ($R' = Me, Et, Ph$). Product **13** was formed along with double bond isomers as the major products (see SI S9 SI Fig. 45–47 for additional details). (b) The dimer conversion (%) over time (s) across 16 hours under dark conditions. Dimer conversion (%) was calculated by integrating 1H resonances corresponding to starting material and dimer products, then computing (dimers/dimers + starting material) \times 100%. (c) ORTEP plot of $[Fe(PhCH=CHCO_2Me)(dmpe)_2]$ **15**, hydrogens have been omitted for clarity and X-ray ellipsoids have been set at 50% probability.

propenyl)-3-ethylglutaric acid dimethyl ester **13** (see SI S9, SI Fig. 46 for further details) similar to findings reported by Waymouth.²⁷ As all products formed from methyl (*E*)-2-pentenoate **11** dimerisation contain an internal alkene, there is no thermodynamic favourability to isomerise to the expected product (*E*),(*Z*)-2-(1-propenyl)-3-ethylglutaric acid dimethyl ester **13**. This contrasts from the isomerisation pathway observed with methyl crotonate **1** which isomerises to the more thermodynamically stable internal conjugated alkene (Scheme 1a, right). Methyl cinnamate **12**, which has no allylic C–H bonds, showed no observable dimerisation after 16 hours in the absence of light irradiation, providing further support for the base-mediated pathway where suitably acidic C–H bonds are present.

Although no dimerisation of methyl cinnamate **12** was recorded under dark conditions, exposure of the same sample to UV irradiation (365 nm) gave rapid conversion to the dimer (*E*),(*Z*)-2-benzylidene-3-phenyl-glutaric acid dimethyl ester **14**. This indicated that only the redox Fe^0/Fe^{II} reductive dimerisation pathway was operating for methyl cinnamate **12** (Scheme 1a, left). Accordingly, $^{31}P\{^1H\}$ NMR spectroscopy showed that the metallacyclopropane iron species

$[(dmpe)_2Fe(PhCH=CHCO_2Me)]$ **15** formed steadily to become the major species after 2 hours. Red crystals deposited from pentane at $-35^\circ C$ were analysed by single crystal X-ray crystallography and identified as complex **15** (Fig. 1c, see SI S7.1 for more details). $[(dmpe)_2Fe(PhCH=CHCO_2Me)]$ **15** was confirmed to be a catalytically active intermediate when used as a catalyst (5 mol%) with methyl crotonate **1** and exposed to UV (365 nm) irradiation for 1 hour, giving the continued formation of (*E*),(*Z*)-2-ethylidene-3-methylpentanedioate **2**, in addition to small amounts of other dimers (see SI S9, SI Fig. 77).

Using methyl crotonate **1** as a benchmark to gain insight into the iron species formed in the light and dark pathways, dimerisation by $[(dmpe)_2FeH_2]$ **3** was monitored using *in situ* LED 1H and $^{31}P\{^1H\}$ NMR spectroscopy³⁷ over a 2 hours period (Fig. 2a) with post-acquisition FID processing.³⁸ A light–dark experiment (Fig. 2a) showed that upon irradiation a large increase in the rate of product formation occurred, whilst stopping irradiation (dark) showed a slower rate of conversion. This suggests that the two mechanisms operate in tandem in the presence of light, with the base-mediated pathway as the major mechanism in the absence of light. Even after complete consumption of $[(dmpe)_2FeH_2]$ **3** in the light–dark reaction,





Fig. 2 (a) Methyl crotonate **1** dimerisation under light (lilac diamond), light-dark (purple triangle) and dark (blue square) conditions. Boxes in light grey are for the light-dark experiment only, representing time points taken where the light source was turned off. Absolute integrals acquired from ^1H NMR spectroscopy with post-acquisition signal-averaging.³⁸ (b) Light-mediated methyl crotonate **1** (pink) dimerisation to (*E*),(*Z*)-2-ethylidene-3-methylpentanedioate **2** (blue) by $[(\text{dmpe})_2\text{FeH}_2]$ **3** pre-catalyst (light blue) showing the formation of intermediate dimethyl 2-ethenyl-3-methylpentanedioate **7** (purple) is iron-catalysed. Absolute integrals acquired from ^1H NMR spectroscopy with post-acquisition signal-averaging.³⁸ (c) Methyl crotonate **1** (pink) dimerisation to (*E*),(*Z*)-2-ethylidene-3-methylpentanedioate **2** (blue) under dark conditions which shows that the intermediate dimethyl 2-ethenyl-3-methylpentanedioate **7** (purple) is not light-dependent. Absolute integrals acquired from ^1H NMR spectroscopy. (d) Decomposition of $[(\text{dmpe})_2\text{FeH}_2]$ **3** to *trans*- $[(\text{dmpe})_2\text{FeH}(\text{CH}_3\text{CH}=\text{CH}-\text{COO}^-)]$ **16**, *trans*- $[(\text{dmpe})_2\text{FeH}(\text{CH}_3\text{O}_2\text{CC}_6\text{H}_{10}\text{COO}^-)]$ **17** and $[(\text{dmpe})_2\text{FeH}]_2(\mu\text{-dmpe})_2^{2+}$ **18**.





Scheme 2 Isomerisation of methyl 3-butenate **19** to methyl crotonate **1** by $[(dmpe)_2FeH_2]$ **3**. Methyl crotonate **1** can then be dimerised by the base-mediated pathway to give the dimer intermediate dimethyl 2-ethenyl-3-methylpentanedioate **7** which itself can be isomerised by $[(dmpe)_2FeH_2]$ **3** to give (E),(Z)-2-ethylidene-3-methylpentanedioate **2**. ^{31}P NMR spectroscopic analysis of the reaction shows that the major iron species is *trans*- $[(dmpe)_2FeH(CH_2CH=CHCO_2Me)]$ **21**, with minor amounts of $[(dmpe)_2FeHY]$ **23**. Minor amounts of $[(dmpe)_2Fe(\eta^2-1)]$ **22** by thermal activation of $[(dmpe)_2FeH_2]$ **3** were also observed.

converted to *trans*- $[(dmpe)_2FeH(CH_3CH=CH-COO^-)]$ **16**. Subsequent exposure of the same sample to irradiation (365 nm) for 20 minutes led to rapid conversion of methyl crotonate **1** to (E),(Z)-2-ethylidene-3-methylpentanedioate **2**, suggesting that *trans*- $[(dmpe)_2FeH(CH_2CH=CHCO_2Me)]$ **21** can undergo light-mediated reductive elimination of methyl crotonate to give $[(dmpe)_2Fe^0]$ **4**.

Under dark conditions, two additional minor iron species were also identified by 1H - ^{31}P HMBC and 1H - ^{13}C HMBC spectroscopy as $[(dmpe)_2Fe(\eta^2-1)]$ **22** (see SI S5.6 for further details) and $[(dmpe)_2FeHY]$ **23** (see SI S5.7 for further details). $[(dmpe)_2Fe(\eta^2-1)]$ **22** was present in minor amounts, presumably formed by thermal activation of $[(dmpe)_2FeH_2]$ **3**.⁴¹ Four chemically inequivalent ^{31}P NMR resonances were observed which did not correspond to any hydride resonance, and were tentatively assigned as the metallacyclopropane complex $[(dmpe)_2Fe(\eta^2-1)]$ **22**. *trans*- $[(dmpe)_2FeHY]$ **23** was present as a minor iron species which increased in absolute intensity across 16 hours. Full assignment of *trans*- $[(dmpe)_2FeHY]$ **23** was not possible: it was initially assumed that Y was enolate **I**, however no matching peaks in the 1H NMR spectra were found to support this.^{42–44} On the basis of the kinetic data, it was proposed that *trans*- $[(dmpe)_2FeHY]$ **23** is either a short-lived intermediate or a coordination complex which does not play a major role in methyl crotonate dimerisation.

$^{31}P\{^1H\}$ NMR spectra obtained during *in situ* monitoring of methyl crotonate **1** under light and dark dimerisation

conditions both showed several iron species (Fig. 3). Under irradiation, a majority of the pre-catalyst $[(dmpe)_2FeH_2]$ **3** was rapidly consumed presumably to give $[(dmpe)_2Fe^0]$ **4**, which was not observed in accordance with previous reports.⁴⁵ Under irradiation, a majority of $[(dmpe)_2FeH_2]$ **3** was converted to $[(dmpe)_2Fe(\eta^2-1)]$ **22** after 20 minutes by $^{31}P\{^1H\}$ NMR spectroscopy. Extensive isolation studies of $[(dmpe)_2Fe(\eta^2-1)]$ **22** gave single yellow crystals suitable for X-ray diffraction obtained from a saturated solution of pentane at -35 °C (see SI S7.4 for further details). Analysis of $[(dmpe)_2Fe(\eta^2-1)]$ **22** confirmed an η^2 -alkene coordination and a C3–C5 bond length of 1.448(2) Å (Fig. 4a); this is significantly longer than similar uncoordinated activated alkenes with bond lengths of 1.32–1.37 Å.^{46,47} The Dewar–Chatt–Duncanson model suggests that the bond elongation is more typical of $C(sp^3)$ character, however the bond angles varied between 110 and 120° suggesting significant disruption of the double bond and that both alkenyl carbons lie between $C(sp^2)$ and $C(sp^3)$ hybridisation. Comparing the metallocyclopropane Fe–C or C–C bonds in $[(dmpe)_2Fe(\eta^2-1)]$ **22** and $[(dmpe)_2Fe(PhCH=CHCO_2Me)]$ **15** shows no significant difference in bond lengths or bond angles, indicating the metallocyclopropane carbons are between $C(sp^2)$ and $C(sp^3)$ hybridisation in both cases. This suggests that the same type of metallocyclopropane intermediate forms from $[(dmpe)_2FeH_2]$ **3** and methyl crotonate **1** or methyl cinnamate **12**. $[(dmpe)_2Fe(\eta^2-1)]$ **22** was assumed to be the major metallocyclopropane product as no $[(dmpe)_2FeH(CH_3CH=CCO_2Me)]$ **5** or





Fig. 3 (a) *In situ* monitoring by $^{31}\text{P}\{^1\text{H}\}$ NMR spectroscopy with post-acquisition FID processing showing different iron species formed under light conditions of methyl crotonate **1** dimerisation.³⁸ (b) *In situ* monitoring by $^{31}\text{P}\{^1\text{H}\}$ NMR spectroscopy showing different iron species formed under dark conditions.

hydrometallation product $[(\text{dmpe})_2\text{Fe}(\text{CH}_3\text{CH}=\text{CCO}_2\text{Me})(\text{CH}_3\text{-CH}_2\text{-CHCO}_2\text{Me})]$ **6** (Scheme 1) was observed by $^{31}\text{P}\{^1\text{H}\}$ NMR. Under dark conditions, minor peaks of $[(\text{dmpe})_2\text{Fe}(\eta^2\text{-1})]$ **22** were observed to increase throughout monitoring, suggesting thermal activation of methyl crotonate **1** by $[(\text{dmpe})_2\text{FeH}_2]$ **3**.⁴¹ It is possible that a catalytically active species was formed by deprotonation of the allylic methyl group of $[(\text{dmpe})_2\text{Fe}(\eta^2\text{-1})]$ **22** by $[(\text{dmpe})_2\text{FeH}_2]$ **3**, as iron coordination can dramatically reduce the $\text{p}K_{\text{a}}$ of the $\text{C}(\text{sp}^3)\text{-H}$ bond.^{41,48,49} However, the higher rate of reaction under light conditions suggests that $[(\text{dmpe})_2\text{Fe}(\eta^2\text{-1})]$ **22** is predominantly consumed in the light-dependent pathway (Scheme 1a). Under dark conditions, the absolute concentration of $[(\text{dmpe})_2\text{Fe}(\eta^2\text{-1})]$ **22** is highest at the end of the reaction which suggests that it is not a catalytically active species in this case. Further $^{31}\text{P}\{^1\text{H}\}$ NMR spectroscopic analysis showed rapid conversion from $[(\text{dmpe})_2\text{FeH}_2]$ **3** to $[(\text{dmpe})_2\text{Fe}(\eta^2\text{-1})]$ **22** upon irradiation in the presence of methyl crotonate **1**, with $[(\text{dmpe})_2\text{Fe}(\eta^2\text{-1})]$ **22** being the major catalytically active species present after 1000 seconds, before gradually being consumed. ^1H NMR spectroscopic analysis showed the gradual formation of (*E*),(*Z*)-2-ethylidene-3-methylpentanedioate **2** across the same period (see SI S9 SI

Fig. 92 for further details), providing further support for the catalytic activity of $[(\text{dmpe})_2\text{Fe}(\eta^2\text{-1})]$ **22** under light-mediated conditions.

Decomposition products were also identified: $\{[(\text{dmpe})_2\text{FeH}_2(\mu\text{-dmpe})]^{2+}$ **18** was characterised using a diagnostic resonance at δ 14.4 ppm in the $^{31}\text{P}\{^1\text{H}\}$ NMR spectrum, which matched reports from Field and co-workers.³⁹ Absolute integrals assigned to $\{[(\text{dmpe})_2\text{FeH}_2(\mu\text{-dmpe})]^{2+}$ **18** rose rapidly until approximately 2000 seconds under both light and dark conditions, and increased more gradually thereafter (Fig. 3). The second decomposition product, which was the dominant iron species observed by $^{31}\text{P}\{^1\text{H}\}$ NMR at the end of the irradiated reaction, was found to be *trans*- $[(\text{dmpe})_2\text{FeH}(\text{CH}_3\text{CH}=\text{CHCOO}^-)]$ **16**, which was confirmed by single crystal X-ray diffraction (Fig. 4b). This indicated that ester demethylation of methyl crotonate **1** by $[(\text{dmpe})_2\text{Fe}^0]$ **4** was a significant decomposition pathway of catalytic species.^{24,50} While the demethylation mechanism remains unclear, *trans*- $[(\text{dmpe})_2\text{FeCl}_2]$ activated by sodium 2-ethylhexanoate has been reported to demethylate methoxy-substituted arenes,²⁴ and iron-containing enzymes such as cytochrome P450 are known to demethylate other substrates, including lignin.^{51,52} Here, the significant





Fig. 4 ORTEP plots of (a) $[(\text{dmpe})_2\text{Fe}(\eta^2\text{-1})]$ **22**. (b) $\text{Trans}-[(\text{dmpe})_2\text{FeH}(\text{CH}_3\text{CH}=\text{CH}-\text{COO}^-)]$ **16**. (c) $\text{Trans}-[(\text{dmpe})_2\text{FeH}(\text{CH}_3\text{O}_2\text{CC}_6\text{H}_{10}\text{COO}^-)]$ **17**. (d) $[(\text{dmpe})_5\text{Fe}_2]$ **26**. Iron, carbon, phosphorus, oxygen and hydride atoms on the molecular structures are coloured orange, grey, yellow, red and white respectively. Hydrogens have been omitted for clarity and thermal ellipsoids have been set at 50% probability.

formation of $\text{trans}-[(\text{dmpe})_2\text{FeH}(\text{CH}_3\text{CH}=\text{CH}-\text{COO}^-)]$ **16** showed no major hindrance on the rate of reaction, suggesting that at 5 mol% catalyst loading there was sufficient $[(\text{dmpe})_2\text{FeH}_2]$ **3** present for the reaction to proceed. Crotonic acid **24** was observed in trace amounts suggesting that some $\text{trans}-[(\text{dmpe})_2\text{FeH}(\text{CH}_3\text{CH}=\text{CH}-\text{COO}^-)]$ **16** decomposed to elemental iron. Separate investigations reacting $[(\text{dmpe})_2\text{FeH}_2]$ **3** with crotonic acid **24** yielded a red solution containing a complex mixture of iron complexes. Red crystals characterised by $^1\text{H}-^{31}\text{P}$ HMBC and $^1\text{H}-^{13}\text{C}$ HMBC were identified as $\text{trans}-[(\text{dmpe})_2\text{Fe}(\text{CH}_3\text{CH}=\text{CH}-\text{COO}^-)_2]$ **25** (see SI S6.5 and S9 SI Fig. 78–80). Complex **25** was catalytically inactive in the presence of methyl crotonate **1**, in the presence and absence of irradiation (for further details see SI S9, SI Fig. 81).⁵³ During *in situ* monitoring of methyl crotonate **1** dimerisation, no spectroscopic resonances corresponding to $\text{trans}-[(\text{dmpe})_2\text{Fe}(\text{CH}_3\text{CH}=\text{CH}-\text{COO}^-)_2]$ **25** were observed, suggesting that catalyst decomposition to $\text{trans}-[(\text{dmpe})_2\text{FeH}(\text{CH}_3\text{CH}=\text{CH}-\text{COO}^-)]$ **16**, $\text{trans}-[(\text{dmpe})_2\text{FeH}(\text{CH}_3\text{O}_2\text{CC}_6\text{H}_{10}\text{COO}^-)]$ **17** and $[(\text{dmpe})_2\text{FeH}_2(\mu\text{-dmpe})]^{2+}$ **18** was more likely.

Further investigations were conducted by irradiating $[(\text{dmpe})_2\text{FeH}_2]$ **3** in the presence of product (*E*),(*Z*)-2-ethylidene-3-methylpentanedioate **2** to test if competitive insertion to $[(\text{dmpe})_2\text{Fe}^0]$ **4** was inhibiting the reaction. Single crystals of $\text{trans}-[(\text{dmpe})_2\text{FeH}(\text{CH}_3\text{O}_2\text{CC}_6\text{H}_{10}\text{COO}^-)]$ **17** (Fig. 4c) deposited from a saturated pentane solution at -35°C confirmed that



Scheme 3 Using $[(\text{dpe})_2\text{FeH}_2]$ **29** as catalyst for methyl crotonate **1** dimerisation under UV (365 nm) irradiation for 16 hours yielded no (*E*),(*Z*)-2-ethylidene-3-methylpentanedioate **2**. Crystals suitable for X-ray crystallography were grown from the reaction mixture at -35°C and identified as $[(\text{dpe})\text{FeH}(\text{Ph}_2\text{PCH}_2\text{CH}_2\text{PPh}(\text{C}_6\text{H}_4))]^+$ **30**. Iron, carbon and phosphorus atoms on the molecular structures are coloured orange, grey and yellow respectively. Hydrogens have been omitted for clarity and thermal ellipsoids have been set at 50% probability.



demethylation of the conjugated ester in (*E*),(*Z*)-2-ethylidene-3-methylpentanedioate **2** was preferred over either C(sp²)-H oxidative addition or metallacyclopropane formation. This is attributed to the increased steric bulk of trisubstituted alkene (*E*),(*Z*)-2-ethylidene-3-methylpentanedioate **2** disfavoring the formation of an Fe(II) metallocycle compared to disubstituted alkenes methyl crotonate **1** and methyl cinnamate **12** to form $[(\text{dmpe})_2\text{Fe}(\text{PhCH}=\text{CHCO}_2\text{Me})]$ **15** and $[(\text{dmpe})_2\text{Fe}(\eta^2\text{-1})]$ **22**, Fig. 1c and 4a respectively).

Under both light and dark conditions, *trans*- $[(\text{dmpe})_2\text{FeH}(\text{CH}_2\text{CH}=\text{CHCO}_2\text{Me})]$ **21** and *trans*- $[(\text{dmpe})_2\text{FeHY}]$ **23** were observed by ¹H-³¹P HMBC spectroscopy (Fig. 3a and b). Under light conditions *trans*- $[(\text{dmpe})_2\text{FeH}(\text{CH}_2\text{CH}=\text{CHCO}_2\text{Me})]$ **21** was at its highest concentration (0.01 M) at the start of the reaction before being rapidly consumed, whilst under dark conditions *trans*- $[(\text{dmpe})_2\text{FeH}(\text{CH}_2\text{CH}=\text{CHCO}_2\text{Me})]$ **21** grew in absolute concentration to 0.02 M at approximately 5000 seconds

before gradually being consumed. *trans*- $[(\text{dmpe})_2\text{FeHY}]$ **23** was present as a minor iron species in both light and dark conditions, with the highest absolute intensity observed at the start of the experiment and steadily decreasing to trace amounts after approximately 3000 seconds under light conditions. This suggests that *trans*- $[(\text{dmpe})_2\text{FeHY}]$ **23** was either a short-lived intermediate or a coordination complex which does not play a significant role in methyl crotonate dimerisation.

Irradiation of a solution of $[(\text{dmpe})_2\text{FeH}_2]$ **3** in THF-*d*₈ without methyl crotonate **1** at 365 nm for 11 days gave a mixture of iron(0) complexes similar to those reported by Tolman and co-workers.⁵⁴ Specifically, $[(\text{dmpe})_3\text{Fe}_2]$ **26** and $[(\text{dmpe})_3\text{Fe}]$ **27** (Scheme 4) were the major species present; the structure of the former was confirmed by single crystal X-ray diffraction (Fig. 4d and see SI S7.5, for more details).⁵⁵ Addition of methyl crotonate **1** at 5 mol% catalyst loading in the absence of light saw immediate and complete conversion to (*E*),(*Z*)-2-ethylidene-3-



Scheme 4 Speciation of $[(\text{dmpe})_2\text{FeH}_2]$ **3** into multiple structures dependent on the reaction conditions, with potential thermal activation in addition to the light-dependent and light-independent pathways.



synthesis details, characterisation data for compounds including NMR spectroscopy, mass spectrometry, and single crystal X-ray diffraction data. See DOI: <https://doi.org/10.1039/d5sc07490h>.

Acknowledgements

We would like to thank Professor Guy Lloyd-Jones FRS and Dr Luke Britton for insightful contributions. We would also like to thank the EPSRC, the UKRI Future Leaders Fellowship (MR/T042710/1), Johnson Matthey, the Dr Brian R. Phillips Scholarship for Chemical Research, the EPSRC Programme Grant "Boron: Beyond the Reagent" (EP/W007517) and the School of Chemistry for funding this research.

References

- E. Fazekas, P. A. Lowy, M. Abdul Rahman, A. Lykkeberg, Y. Zhou, R. Chamenahalli and J. A. Garden, *Chem. Soc. Rev.*, 2022, **51**, 8793–8814.
- L. Mendez Llatas, E. Sanz Gil, J. Sancho Royo, M. A. Esteruelas Rodrigo, A. M. Lopez de Lama, M. Olivan Esco and E. Onate Rodriguez, Espacenet, EP1325924A1, 2003.
- D. McGuinness, *Dalton Trans.*, 2009, 6915–6923.
- P. Cossee, *J. Catal.*, 1964, **3**, 80–88.
- D. I. Groves, D. Müller, M. Santosh and C.-X. Yang, *GeoGeo*, 2024, 100288.
- J. Ma, C. Feng, S. Wang, K.-Q. Zhao, W.-H. Sun, C. Redshaw and G. A. Solan, *Inorg. Chem. Front.*, 2014, **1**, 14–34.
- Y. Huang, R. Zhang, T. Liang, X. Hu, G. A. Solan and W.-H. Sun, *Organometallics*, 2019, **38**, 1143–1150.
- J. H. P. Cockcroft, G. S. Nichol, J. Holt, J. Smit, J. A. Garden and S. P. Thomas, *ChemCatChem*, 2025, **17**, e00788.
- H. tom Dieck and J. Dietrich, *Angew. Chem., Int. Ed.*, 1985, **24**, 781–783.
- Y. Gao, T. J. Emge, K. Krogh-Jespersen and A. S. Goldman, *J. Am. Chem. Soc.*, 2018, **140**, 2260–2264.
- J. Li, Q. Zhang, X. Hu, Y. Ma, G. A. Solan, Y. Sun and W.-H. Sun, *Appl. Organomet. Chem.*, 2020, **34**, e5254.
- M. A. Cairns and J. F. Nixon, *J. Organomet. Chem.*, 1974, **64**, C19–C21.
- M. McGraw and E. Y. X. Chen, *ACS Catal.*, 2018, **8**, 9877–9887.
- H. Fouilloux and C. M. Thomas, *Macromol. Rapid Commun.*, 2021, **42**, 2000530.
- C. R. Kennedy, M. V. Joannou, J. E. Steves, J. M. Hoyt, C. B. Kovel and P. J. Chirik, *ACS Catal.*, 2021, **11**, 1368–1379.
- P. Meakin, E. Muetterties and J. Jesson, *J. Am. Chem. Soc.*, 1973, **95**, 75–88.
- L. D. Field, A. M. Magill, S. R. Pike, A. J. Turnbull, S. J. Dalgarno, P. Turner and A. C. Willis, *Eur. J. Inorg. Chem.*, 2010, **2010**, 2406–2414.
- M. V. Baker and L. D. Field, *J. Am. Chem. Soc.*, 1986, **108**, 7433–7434.
- M. V. Baker and L. D. Field, *J. Am. Chem. Soc.*, 1987, **109**, 2825–2826.
- M. V. Baker, L. D. Field and D. J. Young, *Appl. Organomet. Chem.*, 1990, **4**, 551–556.
- L. Britton, J. H. Docherty, J. Sklyaruk, J. Cooney, G. S. Nichol, A. P. Dominey and S. P. Thomas, *Chem. Sci.*, 2022, **13**, 10291–10298.
- D. Gerlach, W. Peet and E. Muetterties, *J. Am. Chem. Soc.*, 1972, **94**, 4545–4549.
- T. Dombray, C. G. Werncke, S. Jiang, M. Grellier, L. Vendier, S. Bontemps, J.-B. Sortais, S. Sabo-Etienne and C. Darcel, *J. Am. Chem. Soc.*, 2015, **137**, 4062–4065.
- L. Britton, J. H. Docherty, G. S. Nichol, A. P. Dominey and S. P. Thomas, *Chin. J. Chem.*, 2022, **40**, 2875–2881.
- S. Komiya, T. Ito, M. Cowie, A. Yamamoto and J. A. Ibers, *J. Am. Chem. Soc.*, 1976, **98**, 3874–3884.
- S. H. Komiya, N. H. Oyasato and T. Y. Furukawa, *Bull. Chem. Soc. Jpn.*, 1989, **62**, 4078–4079.
- J. C. A. Flanagan, E. J. Kang, N. I. Strong and R. M. Waymouth, *ACS Catal.*, 2015, **5**, 5328–5332.
- R. H. Morris, *J. Am. Chem. Soc.*, 2014, **136**, 1948–1959.
- K. Abdur-Rashid, T. P. Fong, B. Greaves, D. G. Gusev, J. G. Hinman, S. E. Landau, A. J. Lough and R. H. Morris, *J. Am. Chem. Soc.*, 2000, **122**, 9155–9171.
- J. Madasu, S. Shinde, R. Das, S. Patel and A. Shard, *Org. Biomol. Chem.*, 2020, **18**, 8346–8365.
- C. D. T. Nielsen and J. Burés, *Chem. Sci.*, 2019, **10**, 348–353.
- J. Burés, *Angew. Chem., Int. Ed.*, 2016, **55**, 16084–16087.
- L. A. Hudson, W. Stroek and M. Albrecht, *Dalton Trans.*, 2024, **53**, 14795–14800.
- T. P. Pabst, J. V. Obligacion, É. Rochette, I. Pappas and P. J. Chirik, *J. Am. Chem. Soc.*, 2019, **141**, 15378–15389.
- L. R. Mills, D. Gygi, E. M. Simmons, S. R. Wisniewski, J. Kim and P. J. Chirik, *J. Am. Chem. Soc.*, 2023, **145**, 17029–17041.
- L. Wojnárovits, E. Takács, K. Dajka and S. S. Emmi, *Res. Chem. Intermed.*, 2001, **27**, 847–854.
- Y. Ben-Tal and G. C. Lloyd-Jones, *J. Am. Chem. Soc.*, 2022, **144**, 15372–15382.
- A. Flook and G. C. Lloyd-Jones, *J. Org. Chem.*, 2024, **89**, 16586–16593.
- M. V. Baker, L. D. Field and D. J. Young, *J. Chem. Soc., Chem. Commun.*, 1988, 546–548, DOI: [10.1039/C39880000546](https://doi.org/10.1039/C39880000546).
- P. Jurd, *PhD doctorate*, UNSW, 2018.
- L. D. Field, E. T. Lawrenz, W. J. Shaw and P. Turner, *Inorg. Chem.*, 2000, **39**, 5632–5638.
- P. V. Ramachandran, D. Nicponski and B. Kim, *Org. Lett.*, 2013, **15**, 1398–1401.
- C. Camilletti, D. D. Dhavale, F. Donati and C. Trombini, *Tetrahedron Lett.*, 1995, **36**, 7293–7296.
- X. Chen, Q. Wang and B. Yu, *Chem. Commun.*, 2016, **52**, 12183–12186.
- M. K. Whittlesey, R. J. Mawby, R. Osman, R. N. Perutz, L. D. Field, M. P. Wilkinson and M. W. George, *J. Am. Chem. Soc.*, 1993, **115**, 8627–8637.
- H. Kooijman, J. W. Sprengers, M. J. Agerbeek, C. J. Elsevier and A. L. Spek, *Acta Crystallogr., Sect. E: Struct. Rep. Online*, 2004, **60**, o917–o918.
- X. Wang and L.-Z. Zhang, *Acta Crystallogr., Sect. E: Struct. Rep. Online*, 2012, **68**, o1930.



- 48 Y. Wang, J. Zhu, A. C. Durham, H. Lindberg and Y.-M. Wang, *J. Am. Chem. Soc.*, 2019, **141**, 19594–19599.
- 49 A. Cutler, D. Ehntholt, W. Giering, P. Lennon, S. Raghu, A. Rosan, M. Rosenblum, J. Tancrede and D. Wells, *J. Am. Chem. Soc.*, 1976, **98**, 3495–3507.
- 50 L. D. Field, A. V. George and B. A. Messerle, *J. Chem. Soc., Chem. Commun.*, 1991, 1339–1341, DOI: [10.1039/C39910001339](https://doi.org/10.1039/C39910001339).
- 51 E. S. Ellis, D. J. Hinchey, A. Bleem, L. Bu, S. J. B. Mallinson, M. D. Allen, B. R. Streit, M. M. Machovina, Q. V. Doolin, W. E. Michener, C. W. Johnson, B. C. Knott, G. T. Beckham, J. E. McGeehan and J. L. DuBois, *JACS Au*, 2021, **1**, 252–261.
- 52 M. E. Wolf, D. J. Hinchey, J. E. McGeehan and L. D. Eltis, *J. Biol. Chem.*, 2024, **300**, 107809.
- 53 H. Azizian and R. H. Morris, *Inorg. Chem.*, 1983, **22**, 6–9.
- 54 C. Tolman, S. Ittel, A. English and J. Jesson, *J. Am. Chem. Soc.*, 1978, **100**, 4080–4089.
- 55 P. M. Jurd, H. L. Li, M. Bhadbhade, J. D. Watson and L. D. Field, *J. Organomet. Chem.*, 2022, **961**, 122252.
- 56 A. M. Messinis, T. von Münchow, M. Surke and L. Ackermann, *Nat. Catal.*, 2024, **7**, 273–284.
- 57 G. Hata, H. Kondo and A. Miyake, *J. Am. Chem. Soc.*, 1968, **90**, 2278–2281.
- 58 (a) CCDC 2453128: Experimental Crystal Structure Determination, 2025, DOI: [10.5517/ccdc.csd.cc2nbp5w](https://doi.org/10.5517/ccdc.csd.cc2nbp5w); (b) CCDC 2453129: Experimental Crystal Structure Determination, 2025, DOI: [10.5517/ccdc.csd.cc2nbp6x](https://doi.org/10.5517/ccdc.csd.cc2nbp6x); (c) CCDC 2453130: Experimental Crystal Structure Determination, 2025, DOI: [10.5517/ccdc.csd.cc2nbp7y](https://doi.org/10.5517/ccdc.csd.cc2nbp7y); (d) CCDC 2453131: Experimental Crystal Structure Determination, 2025, DOI: [10.5517/ccdc.csd.cc2nbp8z](https://doi.org/10.5517/ccdc.csd.cc2nbp8z); (e) CCDC 2453132: Experimental Crystal Structure Determination, 2025, DOI: [10.5517/ccdc.csd.cc2nbp90](https://doi.org/10.5517/ccdc.csd.cc2nbp90); (f) CCDC 2453133: Experimental Crystal Structure Determination, 2025, DOI: [10.5517/ccdc.csd.cc2nbpb1](https://doi.org/10.5517/ccdc.csd.cc2nbpb1).

